RSC Advances

PAPER

View Article Online
View Journal | View Issue



Cite this: *RSC Adv.*, 2022, **12**, 12242

# Chemical durability and degradation mechanisms of $CsPbI_3$ as a potential host phase for cesium and iodine sequestration

Keith Bryce, [a] Kun Yang,[a] Yachun Wang[a] and Jie Lian *[ab]

Effective nuclear waste management of radioactive cesium and off-gas iodine from complex waste streams of used fuels is essential for the sustainable development of advanced nuclear fuel cycles. Once cesium and iodine are separated from their respective waste streams, host phases are required to immobilize them into a durable waste form matrix for long-term disposition. The inorganic metal halide perovskite, $CsPbI_3$, has a unique crystal structure capable of incorporating both cesium and iodine simultaneously. Exposure to groundwater in geological repositories is a long-term concern for waste forms, as this may cause corrosion and decrease the waste form's ability to retain radionuclides. In this study, we explore the potential of $CsPbI_3$ perovskite as a promising host phase to incorporate Cs and I, and investigate its chemical durability and degradation mechanisms in an aqueous environment. $CsPbI_3$ was synthesized through a solution-based method and was consolidated into dense pellets by spark plasma sintering. The chemical durability of the $CsPbI_3$ pellets was evaluated by static leaching tests in deionized water at different temperatures of 25, 58, and 90 °C. The elemental release mechanisms and surface alteration of the monolithic $CsPbI_3$ pellets were investigated. Both I and Cs displayed a non-congruent leaching behavior and faster release rates as compared to Pb, particularly at longer leaching durations and higher temperatures. At the initial leaching stage, a $PbI_2$ alteration layer formed on the surface of the pellet due to the rapid release of Cs and I, followed by the formation of a PbI(OH) alteration layer. The activation energies for both dissolution and diffusion controlled mechanisms were determined to be 44.90 kJ $mol^{-1}$ and 45.40 kJ $mol^{-1}$ for Pb, 27.10 kJ $mol^{-1}$ and 40.82 kJ $mol^{-1}$ for I and 24.27 kJ $mol^{-1}$ and 23.86 kJ $mol^{-1}$ for Cs, respectively. These results show a clear decrease in activation energies from Pb to I and Cs, suggesting a preferential release of I and Cs. The solution-based synthesis of $CsPbI_3$ as a host phase for Cs and I and the fundamental understanding of the chemical durability and degradation behavior will be useful for further exploring its application for immobilizing iodine and cesium into final durable waste forms for long-term geological disposition.

Received 24th February 2022
Accepted 1st April 2022

DOI: 10.1039/d2ra01259f

rsc.li/rsc-advances



## 1. Introduction

Effective management and disposal of nuclear wastes are crucial to the development of advanced nuclear fuel cycles. Materials are required for the storage and disposal of radioactive fission products either through chemical reprocessing of used nuclear fuels or direct disposition of wastes in geological repositories.[1–3] Among complex high level waste streams, I-129 is of significant concern for long term disposal due to its long half-life ($t_{1/2} = 1.6 \times 10^7$ years), radiotoxicity, and highly mobile nature, especially when concentrated in a localized geological repository. I-129 is water-soluble, highly environmentally mobile, and can easily enter the biosphere, making it a serious environmental hazard.[4–6] In geological repositories, I-129 is one of the key dose contributors after several hundreds of thousands of years of nuclear waste storage. With an increase in temperature, I-129 becomes increasingly volatile, undergoing oxidation and reduction, and forming soluble salts.[6,7] In addition, radioactive cesium Cs-135 ($t_{1/2} = 2.3 \times 10^6$ years, a β emitter) and Cs-137 ($t_{1/2}$ = 30.08 years, a β/γ emitter) are also problematic radionuclides in terms of waste storage and disposal. Particularly, long-lived Cs-135 is of great concern for the long-term performance of a geological disposal system,[8,9] and the short-lived Cs-137 is a major heat generator for interim storage of nuclear wastes.[10] Similar to iodine, cesium is also highly radiotoxic and water soluble, and needs to be confined in stable and durable matrices.

I-129 may be released after fuel assemblies are removed from the reactor core, usually in gaseous effluents as $I_2$, methyl iodide ($CH_3I$), bound to aerosols,[11] or as off-gas during chemical

[a]*Department of Mechanical, Aerospace and Nuclear Engineering, Rensselaer Polytechnic Institute, NY 12180, USA. E-mail: lianj@rpi.edu; Fax: +1-518-276-6025; Tel: +1-518-276-6081*

[b]*Department of Materials Science & Engineering, Rensselaer Polytechnic Institute, NY 12180, USA*

reprocessing of used fuels.[12,13] Wet scrubbing methods, including alkaline scrubbing,[14] Mercurex process,[15] Iodox process,[16] fluorocarbon solvents,[17] and electrolytic scrubbing,[18] can be used to capture gaseous iodine using a liquid solvent, and the resulting products must be further processed into a solid waste form. The solid adsorbents for iodine capture are usually silver-based compounds such as AgZ (silver exchanged mordenite),[19,20] AgA (silver impregnated alumina)[21] and silver impregnated silica gel,[22,23] and carbon-based solid adsorbents such as coal[24] and graphene.[25] Solid adsorbents remove iodine through the adsorption of iodine onto a solid compound and generally have higher iodine removal efficiencies and are more easily converted into a final waste product. Cesium may be extracted from spent nuclear fuels dissolved in nitric acid using the Fission Product Extraction Processes (FPEX).[26,27] Synthetic zeolite can also be used to capture cesium from the waste streams of the chemical reprocessing.[28,29] The adsorbed iodine after capture from the off-gas streams and extracted cesium from the waste streams of chemical reprocessing must be incorporated into an intermediate host phase or eventually be consolidated into durable solid waste forms for long-term disposition.

Different intermediate host phases or waste forms were proposed for iodine and cesium immobilization and disposal. Garino (2011) suggested the use of AgI and silver-exchanged MOR (Ag-MOR) for iodine immobilization, either through combining it with bismuth–silicon–zinc (Bi–Si–Zn)-oxide glass to form composites or a glass shell structure for storage.[30] However, there are environmental concerns with silver in waste forms for long-term storage as it is commonly reduced in subterranean environments similar to geological repositories, potentially liberating iodine from the waste form.[31] Therefore, the silver-based materials can only serve as intermediate phases, not an ideal waste form material. Ceramic waste forms for iodine immobilization have also been studied, and their chemical durability and the confinement of iodine in ceramic host phases were investigated by leaching experiments. For example, Audubert (1997) proposed a core shell composite with lead-vanadate iodoapatite ($Pb_{10}(VO_4)_6I_2$) as the core and lead orthovanadate ($Pb_3(VO_4)_2$) as the shell, showing a good chemical durability.[32] More recently, Zhang (2019) investigated lead-vanadate iodoapatite ($Pb_{9.85}(VO_4)_6I_{1.7}$), where iodine leaching was conducted in water and 0.1 mol $L^{-1}$ $Na_2CO_3$, NaCl, $Na_2SO_4$, and $Na_3PO_4$ solutions, and high iodine release rates were observed especially in the basic and acidic solutions.[33] There have also been ceramic waste forms proposed for cesium immobilization such as hollandite ($A_xB_yC_{8-y}O_{16}$) which is one of the phases in multiphase Synroc assembly. Wang (2020) investigated the structure and the aqueous durability of a complex hollandite ($[Cs_xBa_y][Fe^{3+}_{2y+x}Ti^{4+}_{8-2y-x}]O_{16}$) ($0.3 \leq x, y \leq 0.75$) in water at 90 °C and observed Cs leaching rates in the order of $10^{-3}$ g $m^{-2}$ $d^{-1}$ after 28 days.[34] Various amounts of Ba, the Cs daughter product, could be accommodated on the Cs site by substituting $Fe^{3+}$ unto the $Ti^{4+}$ site. Hollandite displays great flexibility in its design and low leaching rates and thus is a promising candidate for Cs immobilization.[34,35]

Metal halide perovskites are another class of ceramics and are being investigated for simultaneous iodine and cesium immobilization with very high waste loadings. The metal halide perovskites developed recently have been widely used in the optoelectronic field due to the benefits of having excellent carrier mobility and suitable band gap, without the drawback of sensitive organic compounds found in organic and organic-inorganic hybrid solar cells.[36,37] These perovskites have not been widely researched towards their applications in nuclear waste management. Recently, Yang (2020) investigated the leaching behavior of $Cs_3Bi_2I_9$ in a silica composite (70 wt%) and silica core–shell structure (20 wt% $Cs_3Bi_2I_9$).[38] The glass-bonded perovskite structure displays remarkably high waste loadings and excellent chemical durability, outperforming the state-of-the-art waste form materials for iodine and Cs immobilization. An innovative concept was also reported recently using metal halide perovskite $Cs_2SnCl_6$ as a potential host phase to incorporate alkali metals and halides (e.g., Cs and Cl) separated from complex waste streams associated with the pyro-processing of used fuels or molten salt reactors.[39] The glass-bonded $Cs_2SnCl_6$ was also proposed as an advanced waste form material for chloride-based salt wastes and displayed unprecedented high waste loadings and chemical durability. These pioneering works highlight the immense potential of using inorganic metal halide perovskites either as host phases to immobilize waste elements (particularly alkali metals and halides) or embedded into a glass or ceramic composite for geological disposition.

Analog to $Cs_3BiI_9$ and $Cs_2SnCl_6$ for iodine and Cl incorporation, $CsPbI_3$ is another derivative within the family of metal halide perovskites with rich crystal chemistry and structural flexibility. Fig. 1 shows the crystal structure of the δ-$CsPbI_3$. An ideal perovskite structure would comprise of 8 corner-sharing $[PbI_6]^{-4}$ octahedra forming a cube structure with the 12-coordinated $Cs^+$ cation occupying the central position within the cube.[40] However, the δ-$CsPbI_3$ structure consists of double edge sharing $[PbI_6]^{-4}$ octahedra that are slightly tilted with respect to the ideal perovskite structure and connected by the 9-fold coordinated $Cs^+$ cation. $CsPbI_3$ can be used as a host phase for separating cesium and iodine through a simple solution based approach from the wet scrubbing solution or liquid waste streams from chemical reprocessing, and the waste-loading perovskite host phase can be embedded into the glass or ceramic matrix to form composite waste forms. However, the $CsPbI_3$ faces a similar problem as silver-based host phases, as Pb is also a regulated contaminant according to the Resource Conservation and Recovery Act (RCRA) and could be potentially released from the host phase.

In this study, we investigated the chemical durability and phase degradation behavior of monolithic $CsPbI_3$ as a host phase to incorporate cesium and iodine *via* static leaching tests. Waste element-loaded $CsPbI_3$ powders were synthesized through a scalable solution-based approach by direct precipitation and consolidated into dense pellets using spark plasma sintering (SPS). SPS was used to sinter the $CsPbI_3$ pellets due to its fast and uniform sintering process as well as its improved energy efficiency and reproducibility compared to techniques

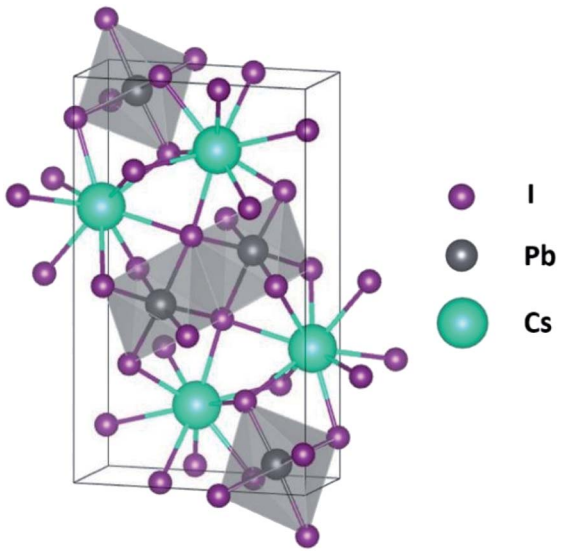


Fig. 1 Illustration of $CsPbI_3$ crystal structure, where Cs and I are indicated by the largest green sphere and smallest purple sphere respectively, and Pb is the grey sphere inside the octahedron.

such as hot press sintering and hot isostatic pressing.[41] Static leaching tests were performed on the sample pellets in deionized water at three different temperatures (25, 50, and 90 °C) to measure the cumulative elemental release. The temperature dependent leaching rates were used to calculate the activation energies of the individual elemental release. Inductively coupled plasma-mass spectroscopy (ICP-MS) measurements were performed to quantify the elemental release in the sampled leachate, and post-leaching characterization was performed on the sample to identify the alteration layers that formed on the surface of the samples and investigate the mechanism of their formation. The results and analysis of these tests should provide a fundamental understanding of chemical durability and degradation mechanisms of the monolithic $CsPbI_3$ perovskite as the host phase of Cs and I, and will be useful for further exploring its application for advanced waste form design in composites.

## 2. Materials and methods

### 2.1 $CsPbI_3$ powder synthesis

The $CsPbI_3$ powders were synthesized by a chemical precipitation method using CsI (99.9%, Sigma Aldrich) and $PbI_2$ (99.9%, Sigma Aldrich) as precursor materials, and methanol was used as the solvent. 1 mmol of CsI was dissolved in 10 mL methanol and heated to ~60 °C in a water bath and 1 mmol of $PbI_2$ powders were dissolved in 4 mL *n*-butyl acetate in a separate beaker. The $PbI_2$ solution was then added to the warm CsI solution and stirred vigorously leading to a spontaneous precipitation of fine yellow $CsPbI_3$ powders. The chemical reaction equation during the process is as follows:

$$CsI + PbI_2 \rightarrow CsPbI_3 \quad (1)$$

The mixture was then stirred for 30 minutes with a stirring speed of 300 rpm to ensure the completion of the reaction in a 60 °C water bath. The solid $CsPbI_3$ precipitates were washed twice using *n*-butyl acetate *via* centrifugation and dried in an oven at 80 °C overnight.

### 2.2 $CsPbI_3$ pellet sintering

$CsPbI_3$ powders were then ground into fine powders and loaded into a 6 mm diameter cylindrical graphite die and consolidated into a dense pellet using SPS (Model 10-3 SPS system, Thermal Tech. LLC, Santa Rosa, CA). A steady flow of argon gas (1 L $min^{-1}$) was used during the sintering process to purge the chamber to avoid oxidation and degradation of $CsPbI_3$ and graphite die. $CsPbI_3$ samples were sintered at five different temperatures (300, 320, 350, 400, and 435 °C) all at 40 MPa for 1 minute to evaluate the effects of temperature on the microstructure of the $CsPbI_3$ pellets. The sintered pellets were then ground by SiC abrasive papers and then polished with 1 μm diamond paste to achieve a mirror finish with anhydrous ethanol acting as the polishing agent. Both top and bottom surfaces were polished as the whole pellets were subjected to leaching conditions.

### 2.3 Crystalline $CsPbI_3$ sample structure and microstructure characterization

The phase composition of the $CsPbI_3$ pellet and synthesized powders were confirmed *via* X-ray diffraction (XRD) using a Panalytical X'Pert Pro system (Westborough, MA, USA) with a copper target ($K\alpha = 0.15406$ nm) and a step size of 0.013°. The physical density of the pellet was measured *via* the Archimedes technique using an Adam analytical scale (Danbury, NY, USA). The microstructures of the pellet samples were examined before and after the leaching experiments *via* digital photography, and scanning electron microscopy (SEM) using a FEI Versa (USA) with an energy-dispersive spectroscopy (EDS) system, conducted with an additional Oxford Instruments INCA detector (Abingdon, UK). Thermogravimetric analysis (TGA) was used to analyze the thermal stability of $CsPbI_3$ using a TGA-Q50 system (TA instruments, New Castle, DE). ~20 mg of $CsPbI_3$ powders were weighed and placed in an alumina crucible, after which the sample was heated at a rate of 20 °C $min^{-1}$ in a steady flow of argon gas at 50 mL $min^{-1}$ until the temperature reached 1100 °C and then cooled at the same rate to 50 °C. A measurement of the Raman shift at the pellet surface was performed before and after the leaching experiment, using a Raman spectrometer with a 514 nm laser, an exposure time of 10 s, and an operating power of 20 mW.

### 2.4 Chemical durability test

Static leaching was conducted on the $CsPbI_3$ pellets sintered at 320 °C, where high-purity 18 MΩ deionized water was used as the leaching agent, following an ASTM C1220 leaching protocol.[42] The pellet was placed in the leaching agent in a sealed PTFE container with the pellet surface area to volume ratio ($S/V$) kept at 5.0 $m^{-1}$ throughout the experiment (initial leachate volume is 46.1 mL based on the sample surface area). The static leaching experiments were conducted at room temperature (RT), 58 and 90 °C, and only 1 mL of leachate was

removed from the PTFE container and replaced with the same amount of fresh leachate to minimize the impact on the concentration at the time intervals of 1, 2, 3, 4, 5, 6, 7, 8, 9, 10 and 68 h. After the experiment, all the leachates collected were filtered and acidified using 5 vol% $HNO_3$ for elemental analysis by ICP-MS. The ICP-MS Varian 820 was used to measure the concentrations of Cs, I, and Pb in the collected leachates to calculate the corresponding cumulative mass release $m_i$ (g m$^{-2}$) using eqn (2).

$$m_i = \frac{C_i V}{S} \quad (2)$$

where $C_i$ is the concentration measured using ICP-MS (g L$^{-1}$), $V$ is the leachate volume (L) and $S$ is the surface area of the pellet (m$^2$). The relation between the cumulative mass release and $t_i$ leaching time (day) is given by an analytical Cote's model[43] for the time evolution of the leaching behavior shown in eqn (3).

$$m(t) = k_1 t + k_2 t^{1/2} + k_3(1 - e^{-k_4 t}) \quad (3)$$

Here, $m(t)$ stands for the cumulative mass leaching out as mg m$^{-2}$. The first term on the right side of the equation, $k_1 t$, represents a linear dissolution behavior. The second and third terms stand for the mass transport by diffusion and species exchange between the matrix surface and solution, respectively. The derivative of eqn (3) allows the determination of the leaching rate, and the parameter $k_1$ represents the long-term rate assuming an infinite leaching duration.

# 3. Results and discussion

### 3.1 Microstructure and thermal stability of as-sintered $CsPbI_3$ pellets under elevated temperatures

Fig. 2f presents the TGA analysis of $CsPbI_3$ powders, which shows a mass loss of greater than 90% at temperatures above 900 °C. The onset temperature of thermal instability for the as-sintered $CsPbI_3$ is approximately 510 °C at which materials start to experience phase decomposition and release of CsI, and almost all the weight was lost around 1000 °C. Therefore, all $CsPbI_3$ pellets were sintered at temperatures below the on-set point of 510 °C to avoid phase degradation during the sintering process. Fig. 2a–e shows SEM images of the fractured surfaces of the $CsPbI_3$ pellets sintered at 300 °C, 320 °C, 350 °C, 400 °C, and 435 °C, respectively, all at 40 MPa for 1 minute. The surfaces appear to be dense and relatively large grains ~2–10 μm can be seen, and grain sizes increase at increased sintering temperatures. While no apparent secondary phases are observed, intergranular cracking is apparent in the samples sintered at 350, 400, and 435 °C. The existence of intergranular cracking within the grain boundary might significantly reduce the grain stability as well as the sample integrity, which could further accelerate the water molecule diffusion into the pellets. Hence, the $CsPbI_3$ pellet sintered at 320 °C was used for the leaching experiment as it was sintered at the highest temperature without intergranular cracking.

### 3.2 Microstructure evolution and surface alteration of $CsPbI_3$ post static leaching

Fig. 3a shows the XRD patterns of the as sintered and post static leached $CsPbI_3$ pellets which can be indexed as the α-$CsPbI_3$ using PDF# 18-0376, and no impurity or secondary phases can be observed from the as-sintered pellet. The XRD patterns of the post leaching pellets at room temperature and 90 °C show strong $PbI_2$ (PDF# 07-0235) peaks and minor PbI(OH) (PDF# 22-0655) peaks, indicating an alteration of the $CsPbI_3$ structure with Cs depletion. Fig. 3b presents the Raman spectrum of the $CsPbI_3$ pellet after the 68 hour leaching test in deionized water. Strong Raman peak shifts are observed at 75 cm$^{-1}$ and 105 cm$^{-1}$, corresponding to the $A1_g$ and $E_g$ stretching modes of $PbI_2$ (ref. 44) respectively, as observed in the pellets leached at room temperature and 90 °C. Fig. 3c shows an optical image of the morphology of the leached surface and Fig. 3d is the EDS analysis of the alteration products. The quantitative EDS

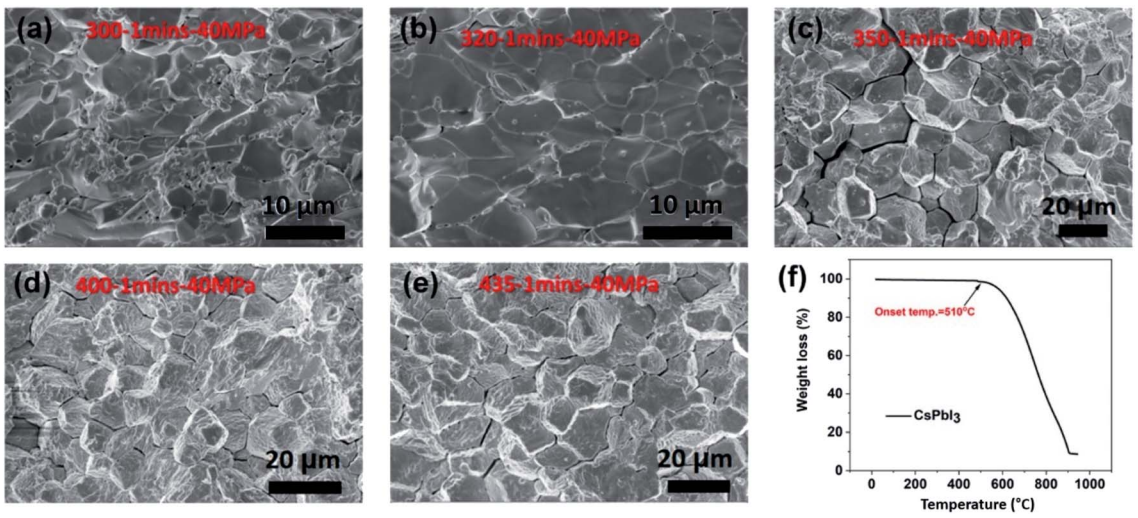


Fig. 2 SEM images showing the fractured surfaces of the SPS densified $CsPbI_3$ pellets for 1 min-40 MPa at (a) 300 °C (b) 320 °C (c) 350 °C (d) 400 °C and (e) 435 °C. (f) Thermogravimetric analysis of $CsPbI_3$ powders from room temperature to 950 °C.

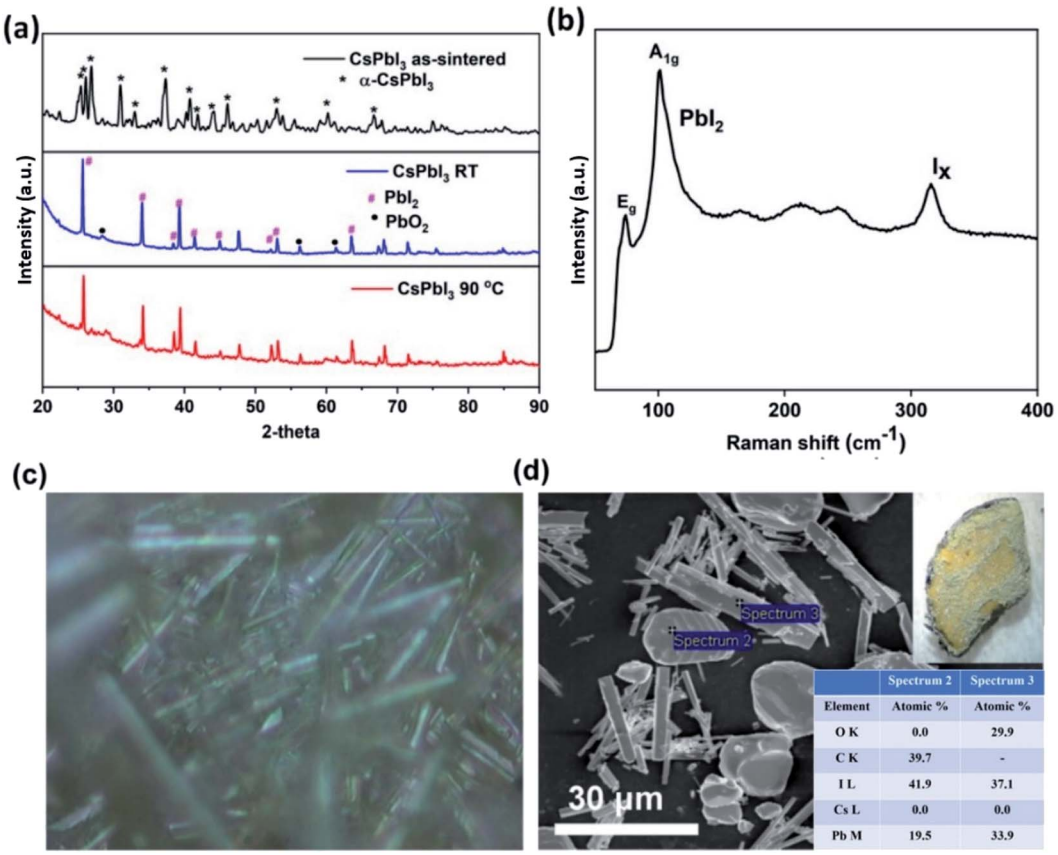


Fig. 3 (a) XRD diffraction patterns of $CsPbI_3$ pellets before and after leaching testing at RT and 90 °C; (b) Raman spectra of the leached pellet leached for 68 hours at 90 °C in deionized water; and (c) optical image of alteration product, (d) SEM image and EDS point analysis at the leached pellet surface post 90 °C leaching for 68 hours.

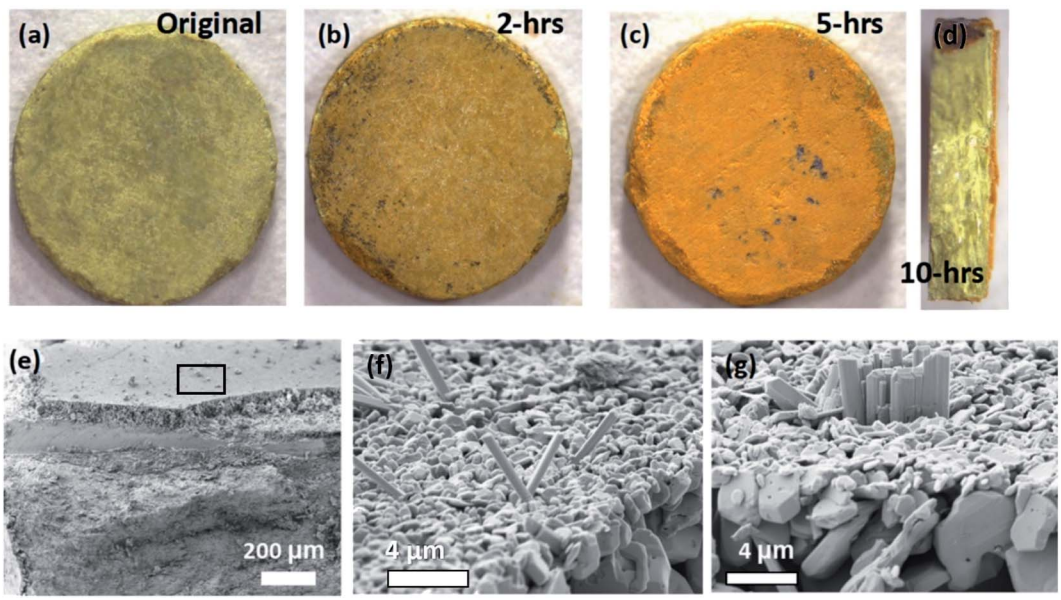


Fig. 4 Optical images showing the morphology, microstructure, and color evolution of the $CsPbI_3$ pellets (a) before leaching; (b) 2 hours; (c) 5 hours; and (d) 10 hours after leaching; (e) an SEM image of the fractured pellet cross-section; and (f and g) SEM images showing surface alteration for the post leaching pellet after 10 hours water exposure.

analysis of spectrum 2 indicates a Pb : I atomic ratio of 1 : 2; while spectrum 3 has a Pb : I : O ratio is approximately 1 : 1 : 1. No Cs is observed from both spectra confirming the depletion of Cs and the retention of Pb and I in the alteration layer, and the alteration products as inferred from spectra 2 and 3 correspond to $PbI_2$ and PbI(OH), respectively.

Fig. 4a–d are optical images showing the degradation morphologies of the $CsPbI_3$ pellets during various stages of the leaching experiments. The pellet changes in color from yellow to dark orange, suggesting severe phase degradation occurred as shown in Fig. 4a–c. The surface of the sample pellet post 10 hours leaching test is covered by an orange alteration layer as shown in Fig. 4d. The alteration layer uniformly covers the surface with a thickness of approximately 100 μm, as demonstrated in the SEM image in Fig. 4e. Fig. 4f–g show the surface microstructure of the altered $CsPbI_3$ pellets, indicating the formation of a loosely-connected alteration layer. From Fig. 4f–g, rod-like particles can be seen on a layer of small polyhedral grains which are layered on top of larger polyhedral grains. Based on the shape of these particles and EDS point analysis, it can be inferred the rod-shaped particles are PbI(OH) and the polyhedral particles are $PbI_2$ based on their crystal structures.

### 3.3 Chemical durability and leaching mechanisms of $CsPbI_3$

The water interaction induces the elemental release which can be quantified in Fig. 5. The elemental release rates (g $m^{-2}$ $h^{-1}$) for Cs, Pb, and I are shown in Fig. 5a, c and e; and the

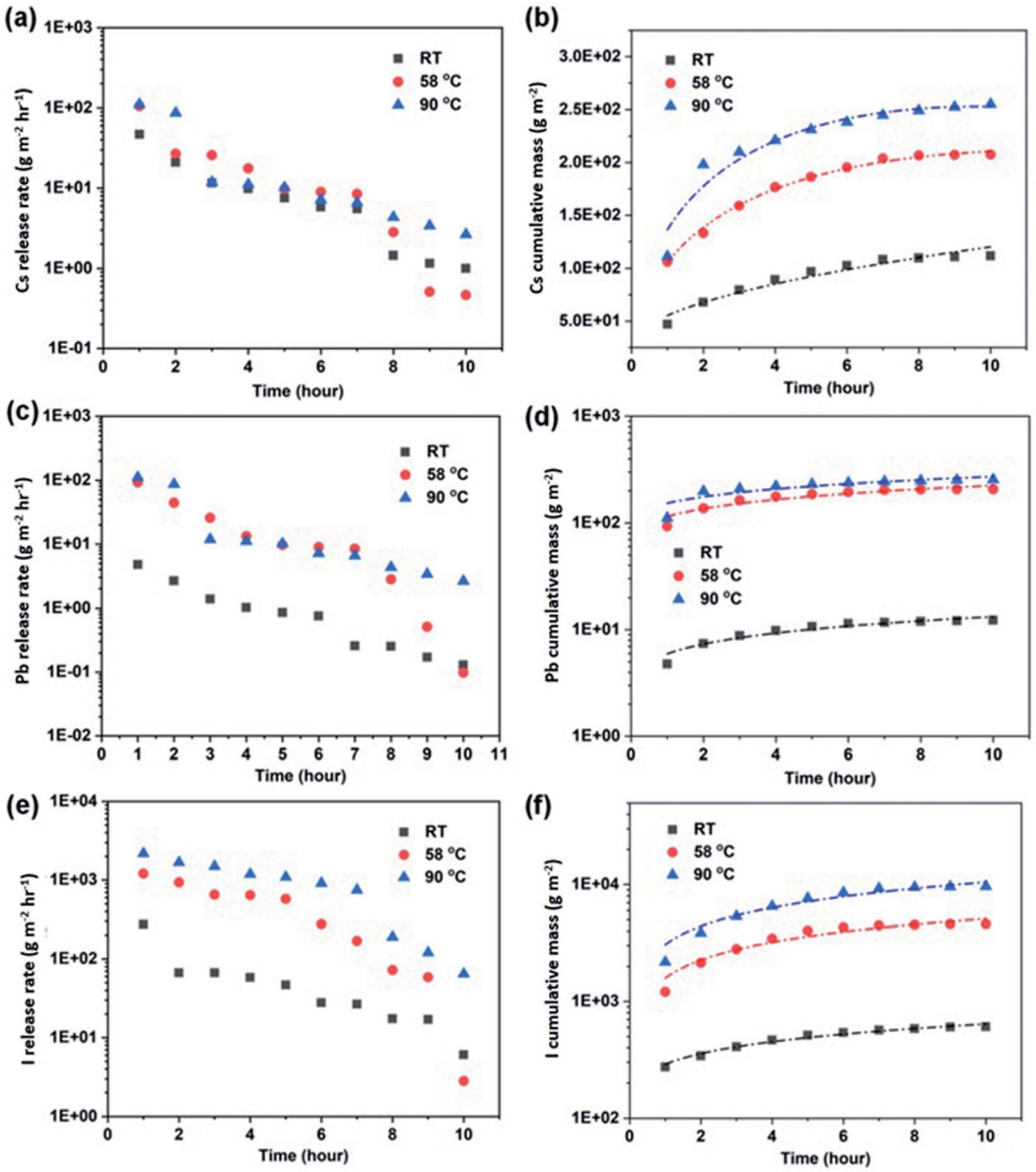


Fig. 5 Elemental release rates (a, c and e) and cumulative mass release rates (b, d, and f) at different temperatures for short-term static leaching for Cs, Pb, and I respectively.

cumulative mass release (g $m^{-2}$) of the corresponding elements are shown in Fig. 5b, d and f. The elemental release rate for $CsPbI_3$ increases when subjected to elevated temperature from 25 °C to 90 °C. For each element, Cs, Pb, and I, the elemental release rates gradually decrease with increased leaching duration, suggesting gradual saturation of the solution, commonly observed for static leaching tests. Moreover, I releases much faster than Cs and Pb, which can be attributed to the weak covalent bonding of Cs–I and Pb–I. Pb has the lowest elemental release rate, probably due to the formation of the surface alteration layer indexed as PbI(OH) (PDF# 22-0655), as confirmed by the XRD profile.

The corresponding atomic ratio can be seen in Fig. 6a–c, and an incongruent leaching mechanism dominates with the I/Cs ratio significantly higher than 3.0 for temperature ranges from 25 °C to 90 °C. The initial leaching of Cs and I can be attributed to the breakage of the weaker Cs–I bonds within the matrix. At higher temperatures, the atomic ratio of I : Cs as shown in Fig. 6b and c increases over time, with the I/Cs atomic ratio being the highest at 90 °C. The I/Cs ratio increases possibly due to the breaking of the stronger $PbI_2$ metal-halide bond. The formation of PbI(OH) alteration layer could lead to the decrease of the I : Cs ratio in the leachate.[45] The initial atomic ratio of Cs/Pb is higher than the stoichiometric ratio of 1 : 1 for $CsPbI_3$ at 25 °C, indicating a lower release rate of Pb, consistent with the stronger covalent bonding of Pb–I compared to Cs–I.[45] The initial rapid dissolution of I and fast release of Cs compared to Pb leads to the formation of $PbI_2$ in the surface alteration layer as inferred from the XRD pattern of the leached surface. $PbI_2$ typically has a lower solubility compared to $CsPbI_3$, which may explain the lower Pb release rate compared to Cs. The bond breakage of Pb–I becomes more severe with time, leading to the change from non-congruent to congruent then back to a non-congruent release mechanism, as evidenced by the Pb/I ratio shown in Fig. 6.

Interestingly, the atomic ratio of Cs/Pb rapidly decreases past the stoichiometric ratio of 1.0 at elevated temperatures from 58 °C to 90 °C, indicating a preferential release of Pb at higher temperatures and longer duration, as the increased temperature and extended duration significantly accelerate the Pb–I bond breakage. The hydrolysis reaction between the $PbI_2$ surface product with water leads to the enhanced release of Pb and the formation of the hydrolysis product PbI(OH). Therefore, the Pb leaching rate increases and surpasses that of Cs as the surface layer is already depleted of Cs. For comparison, a transition from non-congruent to congruent, followed by a non-congruent leaching mechanism can be seen for I/Pb at all temperatures, with the initial I/Pb atomic ratio significantly higher than 3.0, since the covalent bonding of Cs–I is much weaker than Pb–I. The rapid initial release of I and Cs leads to a surface depleted in both elements, which leads to the initial formation of $PbI_2$ at the pellet surface, and the release of I from

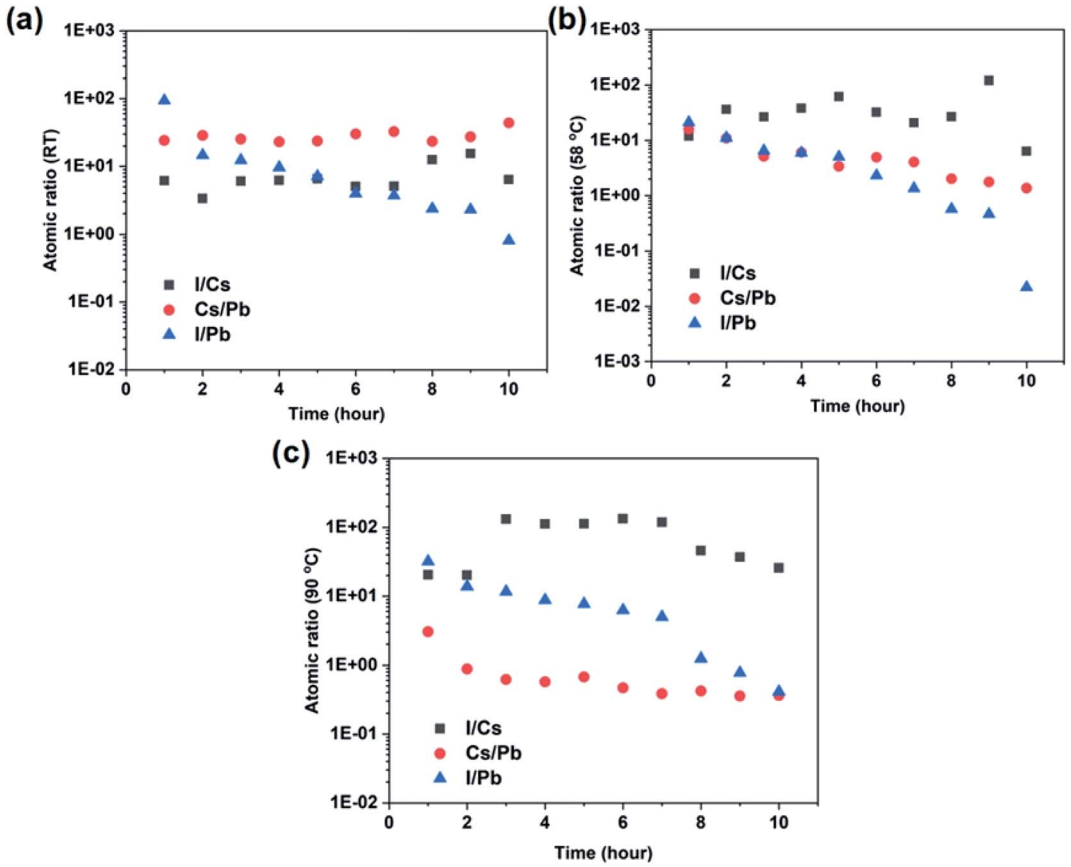


Fig. 6 The atomic ratios of I/Cs, Cs/Pb, and I/Pb in bulk solutions over time at RT (a), 58 °C (b), and 90 °C (c) as measured by ICP-MS.

$PbI_2$ leads to the formation of PbI(OH). The insoluble PbI(OH) (PDF# 22-0655) alteration layer further decreases the release rate of I from the pellet surface.

The rate constants for both dissolution-controlled and diffusion-controlled mechanisms were determined by fitting the cumulative mass concentration using Cote's model with the corresponding fitting curves shown in Fig. 5b, d and f, where the fitting parameters are listed in Table 1. The cumulative mass curves are well fitted using Cote's model as supported by the $R^2$ values on average being higher than 0.9. The results and fitting parameters indicate that the $CsPbI_3$–water interaction behavior can be well explained by three distinct mechanisms, namely, dissolution, surface effect, and diffusion. The dissolution rate and diffusion rate are denoted by $k_1$ and $k_2$ in Table 1, respectively. The cumulative mass curves confirm the gradual reduction of elemental release rates due to the solution saturation during the static leaching test. Particularly for the iodine, this saturation might result in the reprecipitation as evidenced by the reduction in I concentration. With the re-precipitation of the hydrolysis product of PbI(OH) layer on the pellet surface, the elemental releases are continuously reduced (Fig. 5).

A key variable in understanding the diffusion-dominated process is its temperature dependence which may affect the diffusion coefficient in a similar manner to the reaction rate constant.[46] The variation of dissolution and diffusion coefficients with temperature can be well described using the Arrhenius equation below,[47]

$$R(T) = Ae^{-E_a/RT} \quad (4)$$

where $R(T)$ is the dissolution ($k_1$) or diffusion-controlled ($k_2$) rate constants at temperature $T$, which are obtained by fitting the short-term cumulative mass release rates (summarized in Table 2) for each element at all three temperatures (Fig. 5b, d and f) using Cote's model. A is an unknown constant and $E_a$ (kJ) is the apparent activation energy, both of which are independent of temperature, and $R$ is the gas constant ($8.3145 \times 10^{-3}$ kJ $K^{-1}$ $mol^{-1}$). By plotting the natural logarithm of the $k_1$ or $k_2$ rate constant *versus* the inverse of absolute temperature, a linear relationship is obtained (Fig. 7a–b). The slope of this linear relation is then used to calculate the activation energy associated with either the dissolution or diffusion mechanisms for each element, which are listed in Table 3.

Since the elements in the perovskite are not released congruently, it is expected that their activation energies vary accordingly, with Cs having the lowest values of 24.27 kJ $mol^{-1}$ and 23.86 kJ $mol^{-1}$ for dissolution control and diffusion control mechanisms, respectively. This is consistent with the experimental observation in which Cs is preferentially released quickly. Pb has the highest activation energy for both the dissolution and diffusion controlled mechanisms, supporting the observation of the high non-stoichiometric Cs/Pb atomic ratio at room temperature.

In contrast, the activation energy of dissolution for iodine release is significantly lower than that of a diffusion-controlled process, which indicates that elemental diffusion needs to overcome a higher energy barrier before it can occur. This suggests that the iodine release from the $CsPbI_3$ is mainly controlled by the dissolution process upon the bond breaking of Cs–I and Pb–I. The activation energy of dissolution for iodine release is also close to that of Cs, and thus the I/Cs atomic ratio remains relatively close to its stoichiometric value. For Cs and Pb, both dissolution and diffusion activation energies are close, indicating that both processes co-exist to dominate their release rates.

While $CsPbI_3$ has the benefit of over 50 wt% iodine waste loading, compared to other glass and apatite-based waste forms for iodine incorporation investigated by Coulon *et al.* (2017), Chong *et al.* (2018) and Lee *et al.* (2017), the iodine cumulative leaching from $CsPbI_3$ is significantly high.[48–50] Cesium loading is also much higher in the $CsPbI_3$ perovskite than the more commonly studied hollandite structure, and the release rate of Cs is significantly higher than other hollandite waste forms previously studied by Wang *et al.* (2020) and Yang *et al.* (2019).[34,51] Therefore, $CsPbI_3$ itself cannot be used as a durable

Table 1 Fitting parameters for Cs, Pb, and I calculated from the short-term cumulative mass release rates using Cote's model shown in eqn (3)

| | Fitting parameters | *RT* | 58 °C | 90 °C |
|---|---|---|---|---|
| Cs | $k_1$ | 4.6 | 17.9 | 26.0 |
| | $k_2$ | 29.9 | 123.2 | 162.3 |
| | $k_3$ | 25.4 | 0.0 | 0.0 |
| | $k_4$ | 1.0 | 1.0 | 1.0 |
| | $R^2$ | 0.9 | 1.0 | 0.9 |
| Pb | $k_1$ | 0.6 | 1.0 | 17.0 |
| | $k_2$ | 3.4 | 50.8 | 55.2 |
| | $k_3$ | 2.6 | 64.4 | 98.0 |
| | $k_4$ | 1.0 | 1.0 | 1.0 |
| | $R^2$ | 0.9 | 0.9 | 0.9 |
| I | $k_1$ | 16.4 | 52.0 | 115.7 |
| | $k_2$ | 162.0 | 1626.9 | 2947.3 |
| | $k_3$ | 127.5 | 0.0 | 0.0 |
| | $k_4$ | 1.0 | 1.0 | 1.0 |
| | $R^2$ | 1.9 | 0.9 | 1.0 |

Table 2 Dissolution and diffusion-controlled release rates of Cs, Pb, and I at different temperatures

| | Dissolution controlled | | | Diffusion controlled | | |
|---|---|---|---|---|---|---|
| °C | Cs (g $m^{-2}$ $h^{-1}$) | Pb (g $m^{-2}$ $h^{-1}$) | I (g $m^{-2}$ $h^{-1}$) | Cs (g $m^{-2}$ $h^{-1}$) | Pb (g $m^{-2}$ $h^{-1}$) | I (g $m^{-2}$ $h^{-1}$) |
| 25 | 4.6 | 0.6 | 16.4 | 29.9 | 3.4 | 162.0 |
| 58 | 17.9 | 1.0 | 52.0 | 123.2 | 50.8 | 1626.9 |
| 90 | 26.0 | 17.0 | 115.7 | 162.3 | 55.2 | 2947.3 |

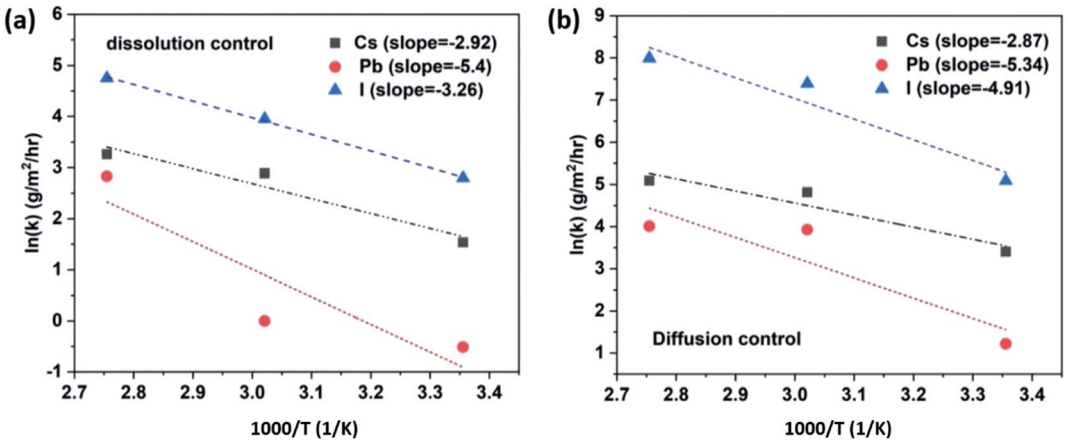


Fig. 7 (a and b) Plots of ln(*k*) *vs.* 1000/*T* (1/*K*), where *k* is the dissolution or diffusion-controlled rate constants determined by fitting of the Cote's model in the of units of g $m^{-2}$ $h^{-1}$.

Table 3 Calculated activation energies, $E_a$, for each element in kJ $mol^{-1}$ based on the Arrhenius equation

| | Dissolution | Diffusion |
|---|---|---|
| Activation energy | kJ $mol^{-1}$ | kJ $mol^{-1}$ |
| Pb | 44.90 | 45.40 |
| I | 27.10 | 40.82 |
| Cs | 24.27 | 23.86 |

waste form matrix for iodine and Cs immobilization because of its lower chemical durability. On the other hand, a high amount of Cs and I can be incorporated into the $CsPbI_3$ structure, after which $CsPbI_3$ can be embedded into either a low temperature glass or a ceramic matrix to form a composite waste form. This concept has already been demonstrated by Yang *et al.* (2021) and may further improve the chemical durability of $CsPbI_3$.[39] Additionally, it is expected that the formation of more water insoluble alteration layers such as $PbI_2$ or PbI(OH) will greatly benefit the retention of iodine and cesium and reduce their release rates. In conjunction with a composite matrix, this could unlock the potential of using inorganic metal halide perovskite as a promising host phase for the immobilization of cesium and iodine.

## 4. Summary

In this study, we explore the $CsPbI_3$ perovskite as a potential host phase for incorporating high amounts of Cs and iodine by investigating its chemical durability and degradation mechanisms. The waste-element loaded α-$CsPbI_3$ can be synthesized from a scalable solution-based approach at a low temperature, and consolidated into a dense pellet at 320 °C *via* SPS without phase decomposition and release of volatile Cs and I. Static leaching testing of the SPS-densified $CsPbI_3$ shows susceptibility of the material to water dissolution, leading to a significant release of waste elements. Mechanistic understandings of non-congruent dissolutions and time evolution of kinetics based on solution chemistry analysis are achieved. This incongruent dissolution mechanism is also evident in the elemental release measurements as Cs is preferentially released compared to Pb at the initial stage of the leaching test at all temperatures. Surface alterations of a $PbI_2$ alteration layer upon initial rapid dissolution of Cs and I occur, followed by a hydrolysis reaction and the formation of PbI(OH) at longer durations. Activation energies for element releases are determined, being the highest for Pb followed by I and Cs. A dissolution dominated mechanism is identified for iodine release through bond-breaking of Pb–I and Cs–I. Advanced materials designs by embedding the waste-loaded host phase with high chemical loadings into a highly chemical durable matrix are required to utilize unique merits of perovskite structures for effective separation and immobilization of problematic Cs and I.

## Conflicts of interest

There are no conflicts to declare.

## Acknowledgements

This work was supported as part of the Center for Performance and Design of Nuclear Waste Forms and Containers (WastePD), an Energy Frontier Research Center (EFRC) funded by the U.S. Department of Energy, Office of Science, Basic Energy Sciences under Award DE-SC0016584.

## References

1 W. Weber, A. Navrotsky, S. Stefanovsky, E. Vance and E. Vernaz, Materials Science of High-Level Nuclear Waste Immobilization, *MRS Bull.*, 2009, **34**(1), 46–53, DOI: 10.1557/mrs2009.12.

2 J. Amoroso, J. Marra, S. D. Conradson, M. Tang and K. Brinkman, Melt processed single-phase hollandite waste forms for nuclear waste immobilization:

$Ba_{1.0}Cs_{0.3}A_{2.3}Ti_{5.7}O_{16}$; A = Cr, Fe, Al, *J. Alloys Compd.*, 2014, **584**, 590–599, DOI: 10.1016/j.jallcom.2013.09.087.

3 R. Ewing, W. Weber and J. Lian, Nuclear waste disposal—pyrochlore ($A_2B_2O_7$):($A_2B_2O_7$): Nuclear waste form for the immobilization of plutonium and "minor" actinides, *J. Appl. Phys.*, 2004, **95**, 5949–5971, DOI: 10.1063/1.1707213.

4 T. Nishimura, T. Sakuragi, Y. Nasu, H. Asano and H. Tanabe, Development of immobilisation techniques for radioactive iodine for geological disposal, in *Mobile fission and activation products in nuclear waste disposal*, La Baule, France, 2007, vol. 16–19, pp. 221–234.

5 J. E. Szecsody, H. P. Emerson, C. I. Pearce, B. N. Gartman, C. Tom Resch and S. A. Di Pietro, *In situ* reductive dissolution to remove Iodine-129 from aquifer sediments, *J. Environ. Radioact.*, 2020, **216**, 106182, DOI: 10.1016/j.jenvrad.2020.106182.

6 E. F. Silva, Geochemistry and environmental mobility of Iodine-129, in *International Nuclear Atlantic Conference*, Rio de Janeiro, Brazil, 2005, p. 4886.

7 B. Grambow, Mobile fission and activation products in nuclear waste disposal, *J. Contam. Hydrol.*, 2008, **102**, 180–186, DOI: 10.1016/j.jconhyd.2008.10.006.

8 P. Laura, Cs-135 Content of Cesium Capsules and Strontium/Cesium Heat Sources, in *Waste Management Conference*, Phoenix, Arizona, USA, 2018, vol. 18–22, p. 18509.

9 M. S. Snow and D. C. Snyder, $^{135}Cs/^{137}Cs$ isotopic composition of environmental samples across Europe: Environmental transport and source term emission applications, *J. Environ. Radioact.*, 2016, **151**, 258–263, DOI: 10.1016/j.jenvrad.2015.10.025.

10 T. Suzuki-Muresan, J. Vandenborre, A. Abdelouas, B. Grambow and S. Utsunomiya, Studies of (Cs, Ba)-hollandite dissolution under gamma irradiation at 95 °C and at pH 2.5, 4.4, and 8.6, *J. Nucl. Mater.*, 2011, **419**, 281–290, DOI: 10.1016/j.jnucmat.2011.09.001.

11 International Atomic Energy Agency, *Radioiodine Removal in Nuclear Facilities, Technical Reports Series No. 201*, IAEA, Vienna, 1980.

12 R. M. Asmussen, J. V. Ryan, J. Matyas, J. V. Crum, J. T. Reiser, N. Avalos, E. M. McElroy, A. R. Lawter and N. C. Canfield, Investigating the Durability of Iodine Waste Forms in Dilute Conditions, *Materials*, 2019, **12**, 686, DOI: 10.3390/ma12050686.

13 R. T. Jubin, D. M. Strachan and N. R. Soelberg, in *Iodine Pathways and Off-Gas Stream Characteristics for Aqueous Reprocessing Plants – A Literature Survey and Assessment*, Idaho National Lab., Idaho, United States, 2013, DOI: 10.2172/1111056.

14 L. L. Burger and R. D. Scheele, in *HWVP Iodine Trap Evaluation*, US Department of Energy, Pacific Northwest National Lab., Richland, Washington, United States, 2004, DOI: 10.2172/15009659.

15 W. Hebel and G. Cottone, in *Management modes for iodine-129*, Harwood Academic Pub, United States, 1982.

16 E. D. Collins and D. E. Benker, in *Iodox process tests in a transuranium element production campaign*, Oak Ridge National Lab., Tennessee, United States, 1979, DOI: 10.2172/6153980.

17 D. Haefner, *Methods of Gas-Phase Capture of Iodine from Fuel Reprocessing Off-Gas: A Literature Survey*, Idaho National Lab., Idaho, United States, 2007, DOI: 10.2172/911962.

18 J. C. Mailen and D. E. Horner, Removal of Radioiodine from Gas Streams by Electrolytic Scrubbing, *Nucl. Technol.*, 1976, **30**, 317–324, DOI: 10.13182/NT76-A31646.

19 T. M. Nenoff, M. A. Rodriguez, N. R. Soelberg and K. W. Chapman, Silver-mordenite for radiologic gas capture from complex streams: Dual catalytic $CH_3I$ decomposition and I confinement, *Microporous Mesoporous Mater.*, 2014, **200**, 297–303, DOI: 10.1016/j.micromeso.2014.04.041.

20 S. H. Bruffey, R. T. Jubin and J. A. Jordan, Capture of Elemental and Organic Iodine from Dilute Gas Streams by Silver-exchanged Mordenite, *Procedia Chem.*, 2016, **21**, 293–299, DOI: 10.1016/j.proche.2016.10.041.

21 M. Kikuchi, M. Kitamura, H. Yusa and S. Horiuchi, Removal of radioactive methyl iodide by silver impregnated alumina and zeolite, *Nucl. Eng. Des.*, 1978, **47**, 283–287, DOI: 10.1016/0029-5493(78)90071-7.

22 N. Mnasri, C. Charnay, L. C. de Ménorval, Y. Moussaoui, E. Elaloui and J. Zajac, Silver nanoparticle-containing submicron-in-size mesoporous silica-based systems for iodine entrapment and immobilization from gas phase, *Microporous Mesoporous Mater.*, 2014, **196**, 305–313, DOI: 10.1016/j.micromeso.2014.05.029.

23 B. J. Riley, J. O. Kroll, J. A. Peterson, J. Matyáš, M. J. Olszta, X. Li and J. D. Vienna, Silver-Loaded Aluminosilicate Aerogels as Iodine Sorbents, *ACS Appl. Mater. Interfaces*, 2017, **9**, 32907–32919, DOI: 10.1021/acsami.7b10290.

24 J. Zhou, S. Hao, L. Gao and Y. Zhang, Study on adsorption performance of coal-based activated carbon to radioactive iodine and stable iodine, *Ann. Nucl. Energy*, 2014, **72**, 237–241, DOI: 10.1016/j.anucene.2014.05.028.

25 S. M. Scott, T. Hu, T. Yao, G. Xin and J. Lian, Graphene-based sorbents for iodine-129 capture and sequestration, *Carbon*, 2015, **90**, 1–8, DOI: 10.1016/j.carbon.2015.03.070.

26 B. J. Mincher, Degradation Issues in Aqueous Reprocessing Systems, *Compr. Nucl. Mater.*, 2012, **5**, 367–388, DOI: 10.1016/B978-0-08-056033-5.00104-X.

27 J. N. Sharma, A. Kumar, V. Kumar, S. Pahan, C. Janardanan, V. Tessi and P. K. Wattal, Process development for separation of cesium from acidic nuclear waste solution using 1,3-dioctyloxycalix[4]arene-crown-6+isodecyl alcohol/*n*-dodecane solvent, *Sep. Purif. Technol.*, 2014, **135**, 176–182, DOI: 10.1016/j.seppur.2014.08.016.

28 P. K. Sinha, P. K. Panicker, R. V. Amalraj and V. Krishnasamy, Treatment of radioactive liquid waste containing cesium by indigenously available synthetic zeolites: A comparative study, *Waste Manag.*, 1995, **15**, 149–157, DOI: 10.1016/0956-053X(95)00014-Q.

29 D. C. Grant, M. C. Skriba, A. K. Saha and D. K. Ploetz, *Design and optimization of a zeolite ion exchange system for the treatment of radioactive wastes*, American Institute of Chemical Engineers, 1988, vol. 84, pp. 13–22.

30 T. J. Garino, T. M. Nenoff, J. L. Krumhansl and D. X. Rademacher, Low-Temperature Sintering Bi–Si–Zn-Oxide Glasses for Use in Either Glass Composite Materials or Core/Shell $^{129}$I Waste Forms, *J. Am. Ceram. Soc.*, 2011, **94**, 2412–2419, DOI: **10.1111/j.1551-2916.2011.04542.x**.

31 V. K. Sharma, J. Filip, R. Zborilb and R. S. Varma, Natural inorganic nanoparticles – formation, fate, and toxicity in the environment, *Chem. Soc. Rev.*, 2015, **44**, 8410–8423, DOI: **10.1039/C5CS00236B**.

32 F. Audubert, J. Carpena, J. L. Lacout and F. Tetard, Elaboration of an iodine-bearing apatite Iodine diffusion into a $Pb_3(VO_4)_2$ matrix, *Solid State Ionics*, 1997, **95**, 113–119, DOI: **10.1016/S0167-2738(96)00570-X**.

33 Z. Zhang, L. Gustin, W. Xie, J. Lian, K. T. Valsaraj and J. Wang, Effect of solution chemistry on the iodine release from iodoapatite in aqueous environments, *J. Nucl. Mater.*, 2019, **525**, 161–170, DOI: **10.1016/j.jnucmat.2019.07.034**.

34 X. Wang, J. Ma, X. Lu, Z. Fang, L. Li, L. Li and Y. Yang, Investigations on the structural evolution and aqueous durability of $[Cs_xBa_y][Fe^{3+}_{2y+x}Ti^{4+}_{8-2y-x}]O_{16}$ ceramics for radioactive cesium storage, *J. Solid State Chem.*, 2020, **288**, 121457, DOI: **10.1016/j.jssc.2020.121457**.

35 Y. Yang, X. Yang, X. Wang, S. Luo, J. Ma and Y. Huang, Chemical evolution effects on phase and microstructure of $[Cs_xBa_y][Ti^{3+}_{2y+x}Ti^{4+}_{8-2y-x}]O_{16}$ ceramic waste forms for radioactive cesium immobilization, *J. Nucl. Mater.*, 2019, **517**, 57–62, DOI: **10.1016/j.jnucmat.2019.02.001**.

36 Y. Zhang, Y. Yang, X. Zhang, T. Wang, L. Nian, Q. Rong, G. Zhou and N. Li, Low-temperature preparation of all-inorganic $CsPbI_3$ perovskite solar cells with ethanediamine as additive, *Org. Electron.*, 2020, **87**, 105940, DOI: **10.1016/j.orgel.2020.105940**.

37 J. Zhang, C. Wang, H. Fu, L. Gong, H. He, Z. Fang, C. Zhou, J. Chen, Z. Chao and J. Fan, Low-temperature preparation achieving 10.95%-efficiency of hole-free and carbon-based all-inorganic $CsPbI_3$ perovskite solar cells, *J. Alloys Compd.*, 2020, **862**, 158454, DOI: **10.1016/j.jallcom.2020.158454**.

38 K. Yang, W. Zhu, S. Scott, Y. Wang, J. Wang, B. J. Riley, J. Vienna and J. Lian, Immobilization of cesium and iodine into $Cs_3Bi_2I_9$ perovskite-silica composites and core-shell waste forms with high waste loadings and chemical durability, *J. Hazard. Mater.*, 2021, **401**, 123279, DOI: **10.1016/j.jhazmat.2020.123279**.

39 K. Yang, W. Zhu, B. J. Riley, J. D. Vienna, D. Zhao and J. Lian, Perovskite-Derived $Cs_2SnCl_6$–Silica Composites as Advanced Waste Forms for Chloride Salt Wastes, *Environ. Sci. Technol.*, 2021, **55**(11), 7605–7614, DOI: **10.1021/acs.est.0c07724**.

40 B. Wang, N. Novendra and A. Navrotsky, Energetics, Structures, and Phase Transitions of Cubic and Orthorhombic Cesium Lead Iodide ($CsPbI_3$) Polymorphs, *J. Am. Chem. Soc.*, 2019, **141**, 14501–14504, DOI: **10.1021/jacs.9b05924**.

41 M. Suárez, A. Fernández, J. Menéndez, R. Torrecillas, H. U. Kessel, J. Hennicke, R. Kirchner and T. Kessel, Challenges and Opportunities for Spark Plasma Sintering: A Key Technology for a New Generation of Materials, in *Sintering Applications*, IntechOpen, 2013, DOI: **10.5772/53706**.

42 ASTM C1220-17, *Standard Test Method for Static Leaching of Monolithic Waste Forms for Disposal of Radioactive Waste*, ASTM International, West Conshohocken, PA, 2017.

43 P. L. Cote, T. W. Constable and A. Moreira, An evaluation of cement-based waste forms using the results of approximately two years of dynamic leaching, *Nucl. Chem. Waste Manage.*, 1987, 7(2), 129–139, DOI: **10.1016/0191-815X(87)90007-6**.

44 P. Wangyang, H. Sun, X. Zhu, D. Yang and X. Gao, Mechanical exfoliation and Raman spectra of ultrathin $PbI_2$ single crystal, *Mater. Lett.*, 2016, **168**, 68–71, DOI: **10.1016/j.matlet.2016.01.034**.

45 The Materials Project, *Materials Data on CsPbI3 by Materials Project*, Lawrence Berkeley National Lab., Berkeley, California, United States, 2020, DOI: **10.17188/1264827**.

46 D. Dougherty and P. Colombo, *Leaching Mechanisms of Solidified Low-Level Waste the Literature Survey; BNL—51899*, Brookhaven National Lab., Upton, New York, United States, 1985.

47 L. W. McKeen, 1 – Introduction to Permeation of Plastics and Elastomers, in *Plastics Design Library, Permeability Properties of Plastics and Elastomers*, ed. Laurence W. McKeen, William Andrew Publishing, 4th edn, 2017, pp. 1–19, ISBN 9780323508599.

48 A. Coulon, A. Grandjean, D. Laurencin, P. Jollivet, S. Rossignol and L. Campayo, Durability testing of an iodate-substituted hydroxyapatite designed for the conditioning of $^{129}$I, *J. Nucl. Mater.*, 2017, **484**, 324–331, DOI: **10.1016/j.jnucmat.2016.10.047**.

49 S. Chong, J. A. Peterson, B. J. Riley, D. Tabada, D. Wall, C. L. Corkhill and J. S. McCloy, Glass-bonded iodosodalite waste form for immobilization of $^{129}$I, *J. Nucl. Mater.*, 2018, **504**, 109–121, DOI: **10.1016/j.jnucmat.2018.03.033**.

50 C. W. Lee, J. Y. Pyo, H. S. Park, J. H. Yang and J. Heo, Immobilization and bonding scheme of radioactive iodine-129 in silver tellurite glass, *J. Nucl. Mater.*, 2017, **492**, 239–243, DOI: **10.1016/j.jnucmat.2017.05.024**.

51 Y. Yang, X. Wang, S. Luo, X. Yang and J. Ma, Stability studies of $[Cs_xBa_y][(Al^{3+},Ti^{3+})2^{y+x}Ti^{4+}_{8-2y-x}]O_{16}$ ceramics for radioactive caesium immobilization, *Ceram. Int.*, 2019, **45**, 7865–7870, DOI: **10.1016/j.ceramint.2019.01.095**.